

## Magnetic structure and electric currents in solar flare regions producing hard X-ray pulsations

I.V. Zimovets<sup>1,2,3</sup> · R. Wang<sup>1</sup> · Y.D. Liu<sup>1,4</sup> ·  
C. Wang<sup>1</sup> · S.A. Kuznetsov<sup>5</sup> ·  
I.N. Sharykin<sup>3,6</sup> · A.B. Struminsky<sup>3,7</sup> ·  
V.M. Nakariakov<sup>8,9</sup>

© Springer ●●●

**Abstract** We present analysis of the magnetic field and vertical electric currents in seven solar flare regions accompanied by the pulsations of hard X-ray (HXR) emission. These flares were studied by Kuznetsov *et al.* (2016) (Paper I), and chosen here because of the availability of the vector magnetograms for their parent active regions (ARs) obtained with the SDO/HMI data. By extrapolation of magnetic field with the non-linear force-free field (NLFFF) method we found

---

✉ I.V. Zimovets  
ivanzim@iki.rssi.ru

- <sup>1</sup> State Key Laboratory of Space Weather, National Space Science Center (NSSC) of the Chinese Academy of Sciences, No.1 Nanertiao, Zhongguancun, Haidian District, Beijing 100190, China
- <sup>2</sup> International Space Science Institute – Beijing (ISSI-BJ), No.1 Nanertiao, Zhongguancun, Haidian District, Beijing 100190, China
- <sup>3</sup> Space Research Institute (IKI) of the Russian Academy of Sciences, Profsoyuznaya str. 84/32, Moscow 117997, Russia
- <sup>4</sup> University of Chinese Academy of Sciences, Beijing 196140, China
- <sup>5</sup> Central Astronomical Observatory at Pulkovo of the Russian Academy of Sciences, Pulkovskoye chaussee 65/1, Saint-Petersburg 196140, Russia
- <sup>6</sup> Institute of Solar-Terrestrial Physics, Russian Academy of Sciences, Siberian Branch, Lermontov st., 126a, Irkutsk p/o box 291 664033, Russia
- <sup>7</sup> Moscow Institute of Physics and Technology (State University), Institutskiy per. 9, Dolgoprudny, Moscow Region 141700, Russia
- <sup>8</sup> Centre for Fusion, Space and Astrophysics, Department of Physics, University of Warwick, Coventry CV4 7AL, UK
- <sup>9</sup> St. Petersburg Branch, Special Astrophysical Observatory, Russian Academy of Sciences, St. Petersburg 196140, Russia

that before each flare there was a magnetic flux rope (MFR) elongated along and above a magnetic polarity inversion line (MPIL) on the photosphere. In two flare regions the sources of the HXR pulsations were located at the footpoints of different magnetic field lines wrapping around the central axis, and constituting an MFR by themselves. In five other flares the parent field lines of the HXR pulsations were not a part of an MFR, but surrounded it in the form of an arcade of magnetic loops. Also, we found that in three out of seven events the sources of the HXR pulsations were located in vicinity of enhanced ( $\gtrsim 10^4$  statampere  $\text{cm}^{-2}$ ) regions of vertical electric currents on the photosphere, having the form of extended ribbons elongated ( $\gtrsim 10$  Mm) mainly along an MPIL. In four remaining events vertical electric currents are concentrated in multiple tiny ( $\lesssim 5$  Mm) islands scattered around the MPIL. In general, the HXR sources are found to locate close but out of the sites of the highest vertical electric currents on the photosphere. There are no significant correlations between intensity of the HXR sources and characteristics of vertical electric currents and magnetic field components (as well as of their evolution in time) on the photosphere beneath the HXR sources. All these observational results are in favor of the concept proposed in Paper I, namely that the HXR pulsations are a consequence of successive episodes of energy release in different magnetic flux tubes (threads) of a complex AR triggered by non-uniform evolution (eruption) of an MFR. This concept is consistent with the “standard” 3D model of solar flares and does not require the presence of MHD waves and oscillations for interpreting HXR pulsations. On the other hand, the findings do not contradict the model of flaring pulsations caused by triggering of spatially and temporally separated magnetic reconnections by a magnetoacoustic wave.

**Keywords:** Flares, Dynamics; Flares, Impulsive Phase; Flares, Relation to Magnetic Field; X-Ray Bursts, Hard

## 1. Introduction

The processes of energy release in solar flares, especially in the impulsive phase, usually are intermittent and non-stationary. This is well evidenced by the presence of multiple peaks (bursts or pulsations) of different amplitudes and duration in the light curves of flare electromagnetic radiation in a broad range of wavelengths: from radio waves to hard X-rays (HXRs), and sometimes even up to gamma-rays (Dennis, 1988; Aschwanden, 2002; McAteer *et al.*, 2007; Kupriyanova *et al.*, 2010; Nakariakov *et al.*, 2010; Simões, Hudson, and Fletcher, 2015).

Despite many years of studying of the flare pulsations, there is no full understanding of the underlying physical mechanisms yet (Nakariakov *et al.*, 2010, 2016; Van Doorselaere, Kupriyanova, and Yuan, 2016). In general, it is believed that the energy in solar flares is released by means of magnetic reconnection (Priest and Forbes, 2002; Shibata and Magara, 2011). Most probably, the flare pulsations are also associated somehow to magnetic reconnection. There are two main groups of the possible models of the long-period pulsations ( $P \gtrsim 1$  s), which

are the main subject of the present work: (1) based on MHD waves and oscillations; (2) based on the so-called “load/unload” mechanisms, *i.e.* spontaneous repetitive magnetic reconnection (Nakariakov and Melnikov, 2009).

The first group of models is more popular because of its relative simplicity, ubiquity of MHD waves and oscillations in the solar atmosphere, and their potential ability to influence all main aspects of the generation of electromagnetic emission in flare regions. In particular, MHD oscillations and waves can be a quasi-periodic trigger/modulator of magnetic reconnection and can influence dynamics of non-thermal particles and plasma in flare loops. Moreover, the MHD oscillations based models are attractive since they could help to diagnose physical parameters of the flaring site (such as plasma density and magnetic field), if there is confidence in the correct choice of the model used (*i.e.* Liu and Ofman, 2014; Nakariakov *et al.*, 2016).

The “load/unload” mechanisms are mainly based on the possibility of the repetitive regimes of energy release in the flare sites through the “bursty” magnetic reconnection (Kliem, Karlický, and Benz, 2000), associated with successive generation of multiple magnetic islands and their subsequent coalescence in an extended quasi-vertical current sheet generated in course of a flare development (Shibata and Tanuma, 2001; Drake *et al.*, 2006; Karlický, Bárta, and Rybák, 2010). There are also several other models belonging to this group and based on different ideas (see, Nakariakov and Melnikov, 2009; Nakariakov *et al.*, 2016; Van Doorselaere, Kupriyanova, and Yuan, 2016, as reviews on this issue).

Possibly, different mechanisms can operate in different flares, due to the wide variety of the physical processes operating there, or different mechanisms can accompany one another in the same flare region. Spatially-resolved observations of sources of the flare pulsations are important for understanding their mechanisms, and for reliable identification of the models used for their interpretation (Grigis and Benz, 2005; Zimovets and Struminsky, 2009; Inglis and Dennis, 2012; Zimovets, Kuznetsov, and Struminsky, 2013; Ning, 2014; Li and Zhang, 2015; Dennis *et al.*, 2017).

Recently, based on the systematic analysis of spatially-resolved observations made by RHESSI (Lin *et al.*, 2002) it was shown that the footpoint (chromospheric) sources of the HXR pulsations (with time differences between successive HXR peaks within the range  $P \approx 8 - 270$  s) in all (29) flares studied are not stationary (anchored) in space — they demonstrate apparent movement in the parent active regions (ARs) from pulsation to pulsation (Kuznetsov *et al.*, 2016, hereafter referred to as Paper I). Based on these observations, it was concluded that the mechanism of the flare HXR pulsations (at least with the characteristic time differences between the successive peaks  $P$  in the considered range) is related to successive triggering of the flare energy release in different magnetic loops of the parent ARs. The triggering mechanism was not directly identified in Paper I. However, based on the fact that more than 85% of the analyzed flares were accompanied by coronal mass ejections (CMEs), *i.e.* were eruptive events, it was hypothesized that a non-uniformly erupting magnetic flux rope (MFR) could act as a trigger of the flare energy release. Successive interaction of different parts of the MFR with certain, spatially separated loops

of the parent active region could lead to apparent motion of the HXR sources and to a series of the HXR pulsations.

The main goal of the present paper is to investigate geometry (structure) of magnetic field in the flare regions studied in Paper I, based on the reconstruction (extrapolation) of the magnetic field in the non-linear force-free field (NLFFF) approximation (Wiegelmann and Sakurai, 2012). The first task is to verify whether MFRs were indeed presented in those ARs prior to the flare onset. The second task is to analyze the spatial relation of MFRs (if present) and the parent magnetic field lines of the sources of the HXR pulsations. This will help to corroborate our hypothesis on the possible role of MFRs in generation of the flare HXR pulsations. The third, by-product, task is to check whether there are correlations (or not) between the intensity of the sources of the HXR pulsations and characteristics of underlying magnetic field and vertical electric currents on the photosphere. The absence of such correlation can be considered as an additional indication that the primary energy release processes responsible for acceleration of electrons (and generation of the HXR pulsations) take place in the corona and do not depend highly on the physical conditions at footpoints of the hosting field lines (flux tubes, loops), as it is suggested in some models (Stepanov and Zaitsev, 2016; Zaitsev, Kronshtadtov, and Stepanov, 2016, and references therein).

## 2. Data analysis

### 2.1. Selection of events

For the following analysis we took the last seven solar flares from the Paper I catalogue (No 23–29): 15-Feb-2011, 07-Jun-2011, 06-Sep-2011, 18-Apr-2014, 22-Oct-2014, 24-Oct-2014, and 09-Nov-2014. This choice is determined by the fact that the parent ARs of these events were observed by the Helioseismic and Magnetic Imager (HMI; Scherrer *et al.*, 2012; Schou *et al.*, 2012) instrument onboard the Solar Dynamics Observatory (SDO), and the vector magnetograms are available for these ARs that is crucial for our goal. We emphasize that this choice is determined only by the availability of these data, and by the events selection criteria in Paper I. No other additional (subjective) criteria are used. The light curves of solar HXR emission detected by RHESSI during these flares are shown in Figure 1.

### 2.2. Extrapolation of magnetic field

For each of seven selected ARs we obtained the pre-flare coronal magnetic field by adopting the non-linear force free field (NLFFF) method as proposed by Wheatland, Sturrock, and Roumeliotis (2000), and extended by Wiegelmann (2004) and Wiegelmann and Inhester (2010). A pre-processing procedure (Wiegelmann, Inhester, and Sakurai, 2006) was employed to remove most of the net force and torque from the data, so that the boundary can be more consistent with the force-free assumption. The NLFFF extrapolation used in our works adopts the

same free parameters as Case-E in (Wiegelmann *et al.*, 2012). As the boundary conditions, we used the Space-weather HMI Active Region Patches (SHARPs) data product described by Bobra *et al.* (2014). This data has a time step of 12 minutes, similar to the standard full-disk SDO/HMI vector magnetograms. We chose the data for the instants of time before the flares, within 2 – 31 minutes prior to the flare onset times according to the GOES data (see Table 1 in Paper I). For the extrapolation in six out of all seven events, we binned the data to  $\approx 1.0''$  per pixel, except for the 09-Nov-2014 event, for which we kept the original pixel size of the HMI magnetograms of  $\approx 0.5''$ . This was done to decrease computational time, though without significant loss of quality. The calculations were performed in rectangular Cartesian coordinates, neglecting the sphericity of the photosphere. The inaccuracies associated with this approach are small, since almost all ARs (except for the 07-Jun-2011 event) are located near the center of the solar disk (see Table 1 in Paper I). Even for the 07-Jun-2011 event, the expected inaccuracies are not critical, because the helio-longitudes and -latitudes of the flare region are less than  $50^\circ$ .

### 2.3. Visualization of the HXR sources and magnetic field lines

To visualize the extrapolated magnetic field and to compare its structure (geometry) with the location of the sources of the HXR pulsations in each event we implemented the following procedure. *First*, we converted the helioprojective-cartesian (HPC) coordinates of the HXR sources to the Stonyhurst heliographic (HG) coordinates using the SolarSoft WCS routines (Thompson, 2006). *Second*, using the formula for the solar differential rotation found by Howard, Harvey, and Forgach (1990), we rotated the HXR sources to the times of the used pre-flare magnetograms to compensate for the time differences between the different data sets. The HXR sources were reconstructed with the use of the RHESSI data and the CLEAN image synthesis algorithm (Hurford *et al.*, 2002) for almost the same time intervals, *i.e.* for the same HXR (25 – 50 keV) pulsations, as in Paper I. For most of the time intervals (corresponding to the HXR pulsations) we used data of all nine RHESSI detectors and the image pixel size is  $1''$ . *Third*, suggesting that the synthesized HXR sources (25 – 50 keV) of the HXR pulsations are located, as usual (Aschwanden, Brown, and Kontar, 2002), in the chromospheric footpoints of the flare magnetic flux tubes (field lines), we found the pixels of the magnetograms corresponding to the brightest pixels of the HXR sources (*i.e.* its brightness maxima). These pixels are used as the starting points for the reconstruction of magnetic field lines in the flaring regions. They are shown by the small colored circles in Figures 2–3. Different colors of the circles (and the field lines started from them) correspond to different time intervals, *i.e.* different HXR pulsations (see Figure 1; almost the same colors were used in Paper I). The field lines are started from the heights of  $\approx 0.7 – 2.2$  Mm above the photosphere to satisfy our aforementioned assumption that the studied HXR sources are located in the chromosphere. The radial component of the magnetic field on the photosphere, the reconstructed magnetic field lines and the corresponding

HXR sources of the HXR pulsations (their centers of maximum brightness) are represented in Figures 2–3 build using the ParaView application<sup>1</sup>.

In addition to the magnetic field lines started from the HXR sources, we also constructed two other sets of field lines. (1) For all ARs studied, except the 15-Feb-2011 and 24-Oct-2011 events (see below), we tried to find localized elongated bundles of helical field lines twisted around a common central axis. Such bundles of field lines can be considered as a reliable approximation of an MFR (*e.g.*, Liu *et al.*, 2016; Guo, Cheng, and Ding, 2017, and references therein). Looking ahead, we note here that we found such bundles of field lines in the central part of all seven considered flare regions. They are shown by the thick light gray field lines (tubes) and also marked by the thick arrows (white or red) in Figures 2–3. We did not try specially to find (and visualize) MFRs for the 15-Feb-2011 and 24-Oct-2011 events, since the reconstructed field lines started from the HXR sources represent such elongated twisted magnetic structure by themselves (see Figure 2(a) and Figure 3(c), where an MFR is indicated also by the thick red arrow), *i.e.* they are different components (threads) of an MFR.

(2) We also reconstructed multiple magnetic field lines started from the main (strongest) magnetic sources (the sunspots’ umbras and penumbras) on the photosphere in all seven ARs studied. This is just to identify better the general magnetic structure of the ARs. These field lines are shown by the thin gray curves in Figures 2–3.

#### 2.4. Characteristics of magnetic field and electric currents beneath the sources of the HXR pulsations

To estimate characteristics of the magnetic field ( $\mathbf{B}$ ) and vertical electric currents ( $j_r$ ) on the photosphere under the sources of the HXR pulsations, and to study possible links (correlations) between these electromagnetic characteristics and intensity of the HXR sources we carried out the following procedure for all the seven flare regions analyzed. (1) We transformed coordinates of all the data used — the pre-flare and post-flare SDO/HMI vector magnetograms (SHARP\_CEA) and the RHESSI HXR images for the time intervals of each HXR pulsation — to the Stonyhurst HG coordinates. This was done with the use of the SolarSoft WCS routines. (2) The HXR images and the post-flare magnetograms were differentially rotated to the observational time of the pre-flare magnetogram. (3) The HG coordinates were transformed to the spherical coordinates ( $r, \theta, \varphi$ ) to simplify the further calculations. (4) For each pixel of the magnetograms we calculated the radial (vertical) electric current density (and its error) using the differential form of the circulation theorem of magnetic induction (*i.e.* of Ampere’s law; in cgs units) as:

$$j_r(\theta, \varphi) = \frac{c}{4\pi} (\nabla \times \mathbf{B})_r = \frac{c}{4\pi} \frac{1}{r \sin \theta} \left( \frac{\partial B_\varphi}{\partial \theta} \sin \theta + B_\varphi \cos \theta - \frac{\partial B_\theta}{\partial \varphi} \right), \quad (1)$$

<sup>1</sup><https://www.paraview.org/>

where  $c$  is the speed of light. Also, we calculated tangential (to the photosphere) and poloidal (*i.e.* azimuthal with respect to  $j_r$ ) components of magnetic field (as well as their errors) respectively as:

$$B_{\text{tan}}(\theta, \varphi) = \sqrt{B_{\theta}^2(\theta, \varphi) + B_{\varphi}^2(\theta, \varphi)} \quad (2)$$

and

$$B_{\text{pol}}(\theta, \varphi) = \frac{2j_r(\theta, \varphi)}{c} \sqrt{\pi S(\theta, \varphi)}, \quad (3)$$

where  $S(\theta, \varphi)$  is a pixel's area. (5) To co-align in space accurately the HXR sources and the maps of magnetic field components, as well as vertical electric current density, we convert the HG coordinates of all the data to the HPC coordinates. (6) Since the resultant HPC coordinate grids are not monotonic and rectangular, we created rectangular monotonic grids and interpolated all the data to these monotonic grids. (7) After this step, we identified each HXR source and found positions of all its pixels, whose HXR fluxes are equal or greater than 90% of the source's maximal flux. (8) Having found such sets of pixels for each HXR source, we calculated the average values of several electromagnetic characteristics on the photosphere below the HXR sources:  $\langle |j_r| \rangle$  — the absolute value of the radial (vertical) electric current density,  $\langle B_{\text{los}} \rangle$  — line-of-sight magnetic field component,  $\langle B_r \rangle$  — radial magnetic field component,  $\langle B_{\text{tan}} \rangle$  — tangential magnetic field component, and  $\langle B_{\text{pol}} \rangle$  — poloidal magnetic field component.

Here we note that we did not take into account the values of  $j_r$  which are below its estimated errors and, at the same time, below three standard deviations ( $3\sigma(j_r^{\text{bckg}}) \approx 10^4$  statampere  $\text{cm}^{-2}$ ) of  $j_r^{\text{bckg}}$  calculated for the quiet-sun regions outside the ARs of interest. Also, we would like to mention that we calculated all electromagnetic characteristics using both the pre-flare (index “0”) and post-flare (index “1”) vector magnetograms. This is helpful to check whether there are some significant changes of electric currents and magnetic field beneath the HXR sources on the photosphere during flares, or not.

The maps of pre-flare electric current density on the photosphere with the superimposed sources of the HXR pulsations are shown in Figures 4–5(left). Here by circles of different colors we show the positions of the brightness maxima of the sources of different HXR pulsations. Right panels in Figures 4–5 show the maps of the parameter called `CONF_DISAMBIG` which identifies the confidence assigned to the final magnetic field disambiguation for each pixel (Bobra *et al.*, 2014). For the patch-wise disambiguated SHARP products, which we used, only three values of 90, 60, or 0 are assigned — from the highest elimination of ambiguity to the lowest one. In our case `CONF_DISAMBIG` can also have some other (close to 90, 60, or 0) values due to the interpolation performed. It can be seen that in the majority of cases (except the 18-Apr-2014 event) the HXR sources are located in the regions of high `CONF_DISAMBIG` values. This provides us with a ground for believing that the estimated values of the electromagnetic characteristics are, in general, reliable.

One can see in Figures 4–5 that in three flares (15-Feb-2011, 06-Sep-2011 and 09-Nov-2014), *i.e.* in 40% of the studied events, the HXR sources are located

in the close vicinity to the localised regions of the enhanced vertical electric current density ( $j_r \gtrsim 10^4$  statampere  $\text{cm}^{-2}$ ) having the shape of the elongated ribbons (with the lengths  $l \geq 10''$ ). However, in four other flares (07-Jun-2011, 18-Apr-2014, 22-Oct-2014 and 24-Oct-2014), *i.e.* in 60% of the studied events, the situation is different. There are no elongated ribbon-shape  $j_r$  structures in these flare regions. Vertical electric currents are concentrated in small ( $l \leq 5''$ ) multiple scattered islands. And there are no obvious spatial correlation between the locations of these  $j_r$ -islands and the positions of the sources of the HXR pulsations.

The total number of sources of the HXR pulsations in all seven studied flares is 246. This amount is quite high for the search for a statistically significant correlation between the intensity of the HXR sources and different electromagnetic characteristics of the regions beneath them, *i.e.* of the footpoints of their parent flux tubes on the photosphere. Figure 6(a) shows the scatter plot of the maximal brightness of the HXR sources ( $\max(I_{\text{HXR}})$ ) and the maximum absolute value of pre-flare vertical electric current density ( $\max(|j_{r,0}|)$ ) below the HXR sources. Figure 6(b), for comparison, shows the scatter plot of the average flux over the HXR sources ( $\langle I_{\text{HXR}} \rangle$ ) and the average absolute value of pre-flare vertical electric current density ( $\langle |j_{r,0}| \rangle$ ) in the regions below the HXR sources. The calculated linear Pearson correlation coefficients ( $cc$ ) are shown in the lower right corners. One can see that there are no significant correlations between the studied parameters. The bottom panels of Figure 6 show the same along the axes of ordinates, and the ratios of the post-flare to pre-flare characteristics of  $j_r$  along the abscissa. No correlations are seen as well. Moreover, the ratios of the post-flare to pre-flare characteristics of  $j_r$  have a value close to 1 in the majority of cases. This indicates that there are no perceptible decrease in the vertical electric currents on the photosphere below the HXR sources during the flares studied. There is even a small indication — the group of scattered points on the right-hand side of Figure 6(d) — that in some cases there is an increase in  $\langle |j_r| \rangle$  during the flare. However, since the amount of these data points is small, and this effect is not seen in Figure 6(c), it can not be considered as a strong and ubiquitous phenomenon for all HXR sources studied (see, *e.g.*, Janvier *et al.*, 2014; Sharykin, Kosovichev, and Zimovets, 2015, where a similar phenomenon is discussed in more detail for a few flares).

Figures 7–8 show analogous scatter plots but made for the different components of the magnetic field on the photosphere beneath the sources of the HXR pulsations. The results are similar (as expected) to the ones discussed above: (1) there are no correlations between different magnetic field components and intensity of the HXR sources; (2) there are no significant changes of the magnetic field components during the studied flares. It is also interesting to note that the estimated poloidal component of magnetic field beneath the HXR sources are, in general, one order of magnitude lower than the radial or tangential components, which have comparable values (see Figure 7).

### 3. Summary of the analysis results, and their discussion

Here we summarize and discuss the main results of the performed analysis of seven flares studied. We remind that these flares were taken from Paper I (Kuznetsov *et al.*, 2016) for the further investigation. They were accompanied by the sequences of HXR bursts (pulsations). These flares were selected from Paper I because they all occurred in the “SDO’s epoch”, *i.e.* the photospheric vector magnetograms are available for their parent ARs for the times just before their onset and after their end. This allowed us to make extrapolation of magnetic field in these ARs in the NLFFF approximation, and to investigate its structure in relation to the sources of the HXR pulsations. This also allowed us to search for correlations between the intensity of the HXR sources and vertical current density (as well as different magnetic field components) beneath them on the photosphere.

#### 3.1. Magnetic flux ropes and the sources of HXR pulsations

Based on the performed extrapolation, first, we found that there is a spatially localized bundle of magnetic field lines twisted around their common axis, and elongated mainly along an MPIL in the core of a parent AR before each flare studied (see Figures 2–3). Such bundles of the intertwined field lines can be considered as a reliable signature of the presence of an MFR (*e.g.*, Schrijver, 2009; Schmieder, Démoulin, and Aulanier, 2013; Liu *et al.*, 2016; Guo, Cheng, and Ding, 2017, and references therein) in these ARs. Second, it can be seen clearly from Figures 2–3 that the sources of different HXR pulsations are located in footpoints of different magnetic field lines. Definitely, different HXR pulsations are emitted from different flux tubes (loops) rather than from a single flare loop. Both these findings are consistent with conclusions made in Paper I (see also Introduction). It should be noted here that magnetic structure of ARs changes during eruption of MFRs and associated flares because of magnetic reconnection. However, we believe that the extrapolated pre-flare magnetic field lines, in general, approximate magnetic structure of the ARs studied quite realistically and reliably.

It is interesting to note that in three out of seven events (namely, 15-Feb-2011, 24-Oct-2014 and 09-Nov-2014), *i.e.* in  $\approx 40\%$  of the flares studied, the reconstructed magnetic field lines initiated from the sources of the HXR pulsations form a twisted MFR (shown by the thick red arrow in Figures 2(a)–3(c,d)) by themselves. These field lines are a part of an MFR — they are some of its individual fibers (or threads). We will call this as case-a. However, in the remaining four events (07-Jun-2011, 18-Apr-2014, 22-Oct-2014 and 24-Oct-2014), *i.e.* in  $\approx 60\%$  of the flares studied, the field lines reconstructed from the HXR sources are not a part of an MFR situated in a parent AR (shown by the thick white arrow in Figures 2(b,c)–3(a,b)). These field lines are located around an MFR in the form of an overlying arcade of magnetic loops (case-b).

The “standard” 3D solar flare model is easily applicable to a magnetic geometry of case-b (Shibata and Magara, 2011; Janvier, Aulanier, and Démoulin, 2015). In this case, the HXR pulsations can be a result of successive episodes

of magnetic reconnection, acceleration of electrons and their precipitation along different magnetic flux tubes (loops) of a magnetic arcade non-uniformly (along its longitudinal axis or an MPIL) stretched by an erupting MFR (see, *e.g.*, discussions in Grigis and Benz, 2005; Liu, Alexander, and Gilbert, 2009; Liu *et al.*, 2010; Nakariakov and Zimovets, 2011). On the other hand, we cannot totally rule out other possibilities. In particular, it is not excluded that successive episodes of magnetic reconnection and particle acceleration (consequently, HXR pulsations) may occur in the interaction regions of an MFR’s outer shells with different surrounding magnetic loops. From Figure 2(b–c) and Figure 3(a) it can be seen that the orientation of the MFR’s field lines (light gray) is different from the orientation of the surrounding field lines hosting the sources of the HXR pulsations (color). Such different orientation of the interacting magnetic flux tubes is a favorable condition for the initiation of magnetic reconnection (*e.g.*, Sakai and de Jager, 1996; Linton, Dahlburg, and Antiochos, 2001). Further observations and modeling are required to confirm or disprove this scenario (see also Netzel *et al.*, 2012; Hassanin and Kliem, 2016).

The “standard” 3D solar flare model is also applicable to the studied flares of case-a. In particular, it was already used successfully by Janvier *et al.* (2014) to interpret the 15-Feb-2011 event (see also Schrijver *et al.*, 2011). The absence of visible HXR sources in the footpoints of the overlying field lines, surrounding an MFR (shown by the thin gray curves in Figures 2–3), may be due to the lower efficiency of magnetic reconnection and electron acceleration in these flux tubes, and insufficient sensitivity of RHESSI. This can also be applicable to the confined flare of 09-Nov-2014, which is not accompanied by a CME (see Table 1 in Paper I). As it was recently shown by Hassanin and Kliem (2016), magnetic reconnection can also occur during a confined eruption of a MFR, both beneath and atop an MFR. Another possibility of the energy release in the 09-Nov-2014 flare, based on 3D reconnection at a separator, was discussed by Li *et al.* (2016).

The discussed concept of generation of HXR (and other wavebands) pulsations does not, in general, require the presence of MHD waves and oscillations, as it is often assumed (see Introduction). In this concept, pulsations are just a result of a triggering of energy release and acceleration of particles in certain different magnetic elements (flux tubes) that are somehow different from the neighbouring magnetic flux tubes, due to non-uniform, essentially 3D, evolution of an MFR in highly inhomogeneous medium of parent ARs, consisting of multitude of magnetoplasma elements with different physical parameters. This may explain why flare pulsations often have rather random character than show quasi-periodic behavior (*e.g.*, Gruber *et al.*, 2011; Inglis, Ireland, and Dominique, 2015; Inglis *et al.*, 2016). On the other hand our results do not contradict the model of the quasi-periodic triggering of magnetic reconnection and a series of localised energy releases by magnetoacoustic waves, developed by Nakariakov and Zimovets (2011). In this scenario the lack of a clear periodicity may be attributed to the complex magnetic field geometry in the flaring active region, which leads to the variation of the magnetoacoustic travel times between the successive acts of the reconnection triggering.

Possible interpretation of the quasi-periodicity within the non-MHD-wave concept was given in Paper I. In the simplest case, this requires the constancy of

an MFR eruption speed ( $v \approx \text{const}$ ) and the presence of spatial inhomogeneity in the physical parameters of surrounding magnetic arcades, with a characteristic spatial scale ( $l \approx \text{const}$ ) along the direction of the MFR motion. In such case, the quasi-period of pulsations can be determined simply as  $P \approx \langle P \rangle \approx l/v \approx \text{const}$ . However, this interpretation has some shortcomings too. First, it is unclear why an MFR should erupt at a constant speed. Second, the nature of the spatial modulation of the inhomogeneous surrounding magnetic structures is also not obvious. There is a possibility that a quasi-periodic modulation may exist along an MFR itself, say, due to some oscillations/waves in it — similar to prominence oscillations (*e.g.*, Oliver and Ballester, 2002; Oliver, 2009). This hypotheses, however, requires further study, and is beyond the scope of the present work. Here we do not study quasi-periodicity of the observed HXR pulsations. This will be done in a separate paper. We would like to note also that the discussed concept does not reject the possibility that other physical processes, in particular, related to MHD waves and oscillations, may also act in flare regions and cause quasi-periodic component of pulsations in some cases. However, our findings indicate an important role played by the MFR in the time variability of the flaring emission.

Geometrical characteristics of the found MFRs (the length of its central axis,  $L_{\text{MFR}}$ , and height of its top above the photosphere,  $H_{\text{MFR}}$ ) are summarized in Table 1. In this Table we also present the number ( $n_p$ ) of significant HXR (25–50 keV) pulsations together with the average time differences ( $\langle P \rangle$ ) between the peaks of successive pulsations, taken from Table 2 of Paper I. There is a weak correlation ( $cc \approx 0.40$ ) between  $n_p$  and  $L_{\text{MFR}}$  (Figure 9(a)). Though the number of data points (only seven) is too small to suggest that this effect indeed takes place, it, in principle, can be interpreted as following. A longer MFR can interact with a higher number of different surrounding magnetoplasma elements (flux tubes, loops, which are somehow different from other elements in this magnetoplasma structure) stacked along its axis and an MPIL during the eruption (or a confined eruption). As it was discussed above, each such interaction may be associated with an episode of energy release and an HXR burst (pulsation) as a result. There is also a weak anti-correlation ( $cc \approx -0.38$ ) between  $\langle P \rangle$  and  $L_{\text{MFR}}$  (Figure 9(c)). We do not consider it as significant, and will not discuss it. Data statistics are insufficient for this conclusion.

The last two columns of Table 1 contain information about the group (see Paper I) and case (see above) of each event. There is no consistency between these two different classifications of the flare regions studied.

### 3.2. Characteristics of electric currents and magnetic field beneath the sources of the HXR pulsations

Our additional task was to estimate characteristics of magnetic field and vertical electric currents on the photosphere beneath the sources of the individual HXR pulsations, and to check whether there are links (correlations) between these “electromagnetic” characteristics, and intensity of the HXR sources. First, we found that there is no obvious spatial correlation between the location of the HXR sources and the regions of enhanced (strong) vertical electric currents

( $j_r \geq j_r^{\text{thr}} = 10^4$  statampere  $\text{cm}^{-2}$ ) on the photosphere (see Figures 4–5). Similar “threshold” levels ( $j_r^{\text{thr}}$ ) were used in some previous works studying the vertical electric currents in flare regions to conditionally separate strong and weak currents (*e.g.*, Moreton and Severny, 1968; Janvier *et al.*, 2014; Musset, Vilmer, and Bommier, 2015; Sharykin, Kosovichev, and Zimovets, 2015). Only in three out of seven flares studied (*i.e.* in  $\approx 40\%$  of the studied cases) the HXR sources were found to be situated in close vicinity to the regions of strong electric currents having the shape of ribbons elongated ( $\gtrsim 10$  Mm) along the MPILs. We emphasize that positions (brightness maxima) of the HXR sources, in general, do not coincide with the places of the strongest currents in these cases. In parent ARs of four remaining flares (*i.e.* in  $\approx 60\%$  of the studied cases) electric currents on the photosphere are mainly concentrated in multiple small ( $\lesssim 5$  Mm), scattered islands (see Figure 4(b) and Figure 5(a–c)). Positions of the brightness maxima of the majority of these HXR sources do not coincide with these  $j_r$ -islands, as in the previous case. This result is consistent with the results of some previous works (*e.g.*, Romanov and Tsap, 1990; de La Beaujardiere, Canfield, and Leka, 1993; Leka *et al.*, 1993; Sharykin, Kosovichev, and Zimovets, 2015) on this subject, namely that the flare HXR sources avoid regions of the highest vertical electric current density on the photosphere, “preferentially occurring adjacent to these current channels” (Li *et al.*, 1997).

We did not find significant correlations between intensity of the HXR sources and vertical electric current density on the photosphere below them (see Figure 6(a–b)). Also, we did not find significant correlations between intensity of the HXR sources and the ratio of post-flare to pre-flare electric current densities below them. Finally, as expected, we did not find significant correlations between intensity of the HXR sources and different components of magnetic field (as well as their changes during the flare) below them (see Figures 7–8).

All these findings indicate that there is no a direct link between vertical electric currents (as well as magnetic field) on the photosphere and the efficiency of energy release and acceleration of electrons in parent magnetic flux tubes (loops), at least, in the flares studied. This is in favor of the “standard” concept (discussed above) that the primary energy release and acceleration of particles take place in the corona rather than in the lower levels of the solar atmosphere as suggested in some models (*e.g.*, Stepanov and Zaitsev, 2016; Zaitsev, Kronshtadtov, and Stepanov, 2016).

#### 4. Conclusion

By means of magnetic field extrapolation in the NLFFF approximation we investigated the magnetic geometry and structure of seven solar flare regions accompanied by HXR pulsations. These flares were chosen from the catalogue in Paper I on the basis of the availability of vector magnetograms for their parent ARs, obtained with the SDO/HMI data. We found that there is an MFR elongated along an MPIL in the core of each AR studied, before each flare. In two flare regions ( $\approx 30\%$ ) the sources of the HXR pulsations are located at the footpoints of different magnetic field lines which are constituent parts of the

MFR. In five remaining flare regions ( $\approx 70\%$ ) the parent field lines of the HXR pulsations are not a part of the MFR, but surround it in the form of an arcade of magnetic loops.

Also, we found that in three events ( $\approx 40\%$ ) the sources of the HXR pulsations are located in the vicinity of enhanced ( $\gtrsim 10^4$  statampere  $\text{cm}^{-2}$ ) regions of vertical electric currents on the photosphere, having the form of extended ribbons elongated ( $\gtrsim 10$  Mm) mainly along an MPIL. In four other events ( $\approx 60\%$ ) vertical electric currents are concentrated in multiple tiny ( $\lesssim 5$  Mm) islands scattered around the parent AR. In general, the HXR sources are close but outside the sites of the highest electric currents on the photosphere. There are no significant correlations between intensity of the HXR sources and characteristics of vertical electric currents and magnetic field components (as well as their changes during the flare) on the photosphere beneath the HXR sources. This indicates that the sites of the primary energy release and acceleration of electrons must be higher in the solar atmosphere.

All these observational results support the concept proposed in Paper I, namely that the HXR pulsations are a consequence of successive episodes of energy release in different magnetic flux tubes (threads) of a complex AR, possibly triggered by non-uniform evolution (eruption) of an MFR. This concept is consistent with the “standard” 3D model of solar flares and does not require the presence of MHD waves and oscillations in flare regions for interpreting the HXR (as well as other wavebands) pulsations. On the other hand, the findings do not contradict the model of flaring pulsations caused by triggering of magnetic reconnections at different spatial locations by a magnetoacoustic wave (Nakariakov and Zimovets, 2011).

**Acknowledgments** This work is based upon the activities of the international science team “Pulsations in solar flares: matching observations and models” supported by the International Space Science Institute – Beijing, China. We are grateful to the RHESSI and SDO/HMI teams, whose data products were used in this study. This study was supported by the British Council via the Institutional Links Programme (Project 277352569 “Seismology of Solar Coronal Active Regions”), by the Russian Foundation for Basic Research (grants No. 15-02-0828, 16-32-50117, 16-02-00328), by the Russian Science Foundation (grant No. 16-12-10448). VMN was partially supported by the HSE Teaching Excellence Initiatives. We are also grateful to the Specialized Research Fund for the State Key Laboratories of China.

## References

- Aschwanden, M.J.: 2002, *Particle Acceleration and Kinematics in Solar Flares, A Synthesis of Recent Observations and Theoretical Concepts*, by Markus J. Aschwanden, Lockheed Martin, Advanced technology Center, Palo Alto, California, U.S.A. Reprinted from *SPACE SCIENCE REVIEWS*, Volume 101, Nos. 1-2 Kluwer Academic Publishers, Dordrecht.
- Aschwanden, M.J., Brown, J.C., and Kontar, E.P.: 2002, *Solar Phys.* **210**, 383.
- Bobra, M.G., Sun, X., Hoeksema, J.T., Turmon, M., Liu, Y., Hayashi, K., Barnes, G., and Leka, K.D.: 2014, *Solar Phys.* **289**, 3549.
- de La Beaujardiere, J.-F., Canfield, R.C., and Leka, K.D.: 1993, *Astrophys. J.* **411**, 378.
- Dennis, B.R.: 1988, *Solar Phys.* **118**, 49.
- Dennis, B.R., Tolbert, A.K., Inglis, A., Ireland, J., Wang, T., Holman, G.D., Hayes, L.A., and Gallagher, P.T.: 2017, *Astrophys. J.* **836**, 84.

- Drake, J.F., Swisdak, M., Che, H., and Shay, M.A.: 2006, *Nature* **443**, 553.
- Grigis, P.C. and Benz, A.O.: 2005, *Astrophys. J.* **625**, L143.
- Gruber, D., Lachowicz, P., Bissaldi, E., Briggs, M.S., Connaughton, V., Greiner, J., van der Horst, A.J., Kanbach, G., Rau, A., Bhat, P.N., Diehl, R., von Kienlin, A., Kippen, R.M., Meegan, C.A., Paciesas, W.S., Preece, R.D., and Wilson-Hodge, C.: 2011, *Astron. Astroph.* **533**, A61.
- Guo, Y., Cheng, X., and Ding, M.D.: 2017, *ArXiv e-prints*, arXiv:1706.05769.
- Hassanin, A. and Kliem, B.: 2016, *Astrophys. J.* **832**, 106.
- Howard, R.F., Harvey, J.W., and Forgach, S.: 1990, *Solar Phys.* **130**, 295.
- Hurford, G.J., Schmahl, E.J., Schwartz, R.A., Conway, A.J., Aschwanden, M.J., Csillaghy, A., Dennis, B.R., Johns-Krull, C., Krucker, S., Lin, R.P., McTiernan, J., Metcalf, T.R., Sato, J., and Smith, D.M.: 2002, *Solar Phys.* **210**, 61.
- Inglis, A.R. and Dennis, B.R.: 2012, *Astrophys. J.* **748**, 139.
- Inglis, A.R., Ireland, J., and Dominique, M.: 2015, *Astrophys. J.* **798**, 108.
- Inglis, A.R., Ireland, J., Dennis, B.R., Hayes, L., and Gallagher, P.: 2016, *Astrophys. J.* **833**, 284.
- Janvier, M., Aulanier, G., and Démoulin, P.: 2015, *Solar Phys.* **290**, 3425.
- Janvier, M., Aulanier, G., Bommier, V., Schmieder, B., Démoulin, P., and Pariat, E.: 2014, *Astrophys. J.* **788**, 60.
- Karlický, M., Bárta, M., and Rybák, J.: 2010, *Astron. Astroph.* **514**, A28.
- Kliem, B., Karlický, M., and Benz, A.O.: 2000, *Astron. Astroph.* **360**, 715.
- Kupriyanova, E.G., Melnikov, V.F., Nakariakov, V.M., and Shibasaki, K.: 2010, *Solar Phys.* **267**, 329.
- Kuznetsov, S.A., Zimovets, I.V., Morgachev, A.S., and Struminsky, A.B.: 2016, *Solar Phys.* **291**, 3385.
- Leka, K.D., Canfield, R.C., McClymont, A.N., de La Beaujardiere, J.-F., Fan, Y., and Tang, F.: 1993, *Astrophys. J.* **411**, 370.
- Li, J., Metcalf, T.R., Canfield, R.C., Wülser, J.-P., and Kosugi, T.: 1997, *Astrophys. J.* **482**, 490.
- Li, T. and Zhang, J.: 2015, *Astrophys. J.* **804**, L8.
- Li, Y., Qiu, J., Longcope, D.W., Ding, M.D., and Yang, K.: 2016, *Astrophys. J.* **823**, L13.
- Lin, R.P., Dennis, B.R., Hurford, G.J., Smith, D.M., Zehnder, A., Harvey, P.R., Curtis, D.W., Pankow, D., Turin, P., Bester, M., Csillaghy, A., Lewis, M., Madden, N., van Beek, H.F., Appleby, M., Raudorf, T., McTiernan, J., Ramaty, R., Schmahl, E., Schwartz, R., Krucker, S., Abiad, R., Quinn, T., Berg, P., Hashii, M., Sterling, R., Jackson, R., Pratt, R., Campbell, R.D., Malone, D., Landis, D., Barrington-Leigh, C.P., Slassi-Sennou, S., Cork, C., Clark, D., Amato, D., Orwig, L., Boyle, R., Banks, I.S., Shirey, K., Tolbert, A.K., Zarro, D., Snow, F., Thomsen, K., Henneck, R., McHedlishvili, A., Ming, P., Fivian, M., Jordan, J., Wanner, R., Crubb, J., Preble, J., Matranga, M., Benz, A., Hudson, H., Canfield, R.C., Holman, G.D., Crannell, C., Kosugi, T., Emslie, A.G., Vilmer, N., Brown, J.C., Johns-Krull, C., Aschwanden, M., Metcalf, T., and Conway, A.: 2002, *Solar Phys.* **210**, 3.
- Linton, M.G., Dahlburg, R.B., and Antiochos, S.K.: 2001, *Astrophys. J.* **553**, 905.
- Liu, C., Lee, J., Jing, J., Liu, R., Deng, N., and Wang, H.: 2010, *Astrophys. J.* **721**, L193.
- Liu, R., Alexander, D., and Gilbert, H.R.: 2009, *Astrophys. J.* **691**, 1079.
- Liu, R., Kliem, B., Titov, V.S., Chen, J., Wang, Y., Wang, H., Liu, C., Xu, Y., and Wiegmann, T.: 2016, *Astrophys. J.* **818**, 148.
- Liu, W. and Ofman, L.: 2014, *Solar Phys.* **289**, 3233.
- McAteer, R.T.J., Young, C.A., Ireland, J., and Gallagher, P.T.: 2007, *Astrophys. J.* **662**, 691.
- Moreton, G.E. and Severny, A.B.: 1968, *Solar Phys.* **3**, 282.
- Musset, S., Vilmer, N., and Bommier, V.: 2015, *Astron. Astroph.* **580**, A106.
- Nakariakov, V.M. and Melnikov, V.F.: 2009, *Space Science Reviews* **149**, 119.
- Nakariakov, V.M. and Zimovets, I.V.: 2011, *Astrophys. J.* **730**, L27.
- Nakariakov, V.M., Inglis, A.R., Zimovets, I.V., Foullon, C., Verwichte, E., Sych, R., and Myagkova, I.N.: 2010, *Plasma Physics and Controlled Fusion* **52**, 124009.
- Nakariakov, V.M., Foullon, C., Myagkova, I.N., and Inglis, A.R.: 2010, *Astrophys. J.* **708**, L47.
- Nakariakov, V.M., Pilipenko, V., Heilig, B., Jelínek, P., Karlický, M., Klimushkin, D.Y., Kolotkov, D.Y., Lee, D.-H., Nisticò, G., Van Doorselaere, T., Verth, G., and Zimovets, I.V.: 2016, *Space Science Reviews* **200**, 75.
- Netz, A., Mrozek, T., Kołomański, S., and Gburek, S.: 2012, *Astron. Astroph.* **548**, A89.
- Ning, Z.: 2014, *Solar Phys.* **289**, 1239.
- Oliver, R.: 2009, *Space Science Reviews* **149**, 175.

- Oliver, R. and Ballester, J.L.: 2002, *Solar Phys.* **206**, 45.
- Priest, E.R. and Forbes, T.G.: 2002, *Astronomy and Astrophysics Review* **10**, 313.
- Romanov, V.A. and Tsap, T.T.: 1990, *Soviet Astronomy* **34**, 656.
- Sakai, J.-I. and de Jager, C.: 1996, *Space Science Reviews* **77**, 1.
- Scherrer, P.H., Schou, J., Bush, R.I., Kosovichev, A.G., Bogart, R.S., Hoeksema, J.T., Liu, Y., Duvall, T.L., Zhao, J., Title, A.M., Schrijver, C.J., Tarbell, T.D., and Tomczyk, S.: 2012, *Solar Phys.* **275**, 207.
- Schmieder, B., Démoulin, P., and Aulanier, G.: 2013, *Advances in Space Research* **51**, 1967.
- Schou, J., Scherrer, P.H., Bush, R.I., Wachter, R., Couvidat, S., Rabello-Soares, M.C., Bogart, R.S., Hoeksema, J.T., Liu, Y., Duvall, T.L., Akin, D.J., Allard, B.A., Miles, J.W., Rairden, R., Shine, R.A., Tarbell, T.D., Title, A.M., Wolfson, C.J., Elmore, D.F., Norton, A.A., and Tomczyk, S.: 2012, *Solar Phys.* **275**, 229.
- Schrijver, C.J.: 2009, *Advances in Space Research* **43**, 739.
- Schrijver, C.J., Aulanier, G., Title, A.M., Pariat, E., and Delannée, C.: 2011, *Astrophys. J.* **738**, 167.
- Sharykin, I.N., Kosovichev, A.G., and Zimovets, I.V.: 2015, *Astrophys. J.* **807**, 102.
- Shibata, K. and Magara, T.: 2011, *Living Reviews in Solar Physics* **8**, 6.
- Shibata, K. and Tanuma, S.: 2001, *Earth, Planets, and Space* **53**, 473.
- Simões, P.J.A., Hudson, H.S., and Fletcher, L.: 2015, *Solar Phys.* **290**, 3625.
- Stepanov, A.V. and Zaitsev, V.V.: 2016, *Geomagnetism and Aeronomy* **56**, 952.
- Thompson, W.T.: 2006, *Astron. Astroph.* **449**, 791.
- Van Doorselaere, T., Kupriyanova, E.G., and Yuan, D.: 2016, *Solar Phys.* **291**, 3143.
- Wheatland, M.S., Sturrock, P.A., and Roumeliotis, G.: 2000, *Astrophys. J.* **540**, 1150.
- Wiegmann, T.: 2004, *Solar Phys.* **219**, 87.
- Wiegmann, T. and Inhester, B.: 2010, *Astron. Astroph.* **516**, A107.
- Wiegmann, T. and Sakurai, T.: 2012, *Living Reviews in Solar Physics* **9**, 5.
- Wiegmann, T., Inhester, B., and Sakurai, T.: 2006, *Solar Phys.* **233**, 215.
- Wiegmann, T., Thalmann, J.K., Inhester, B., Tadesse, T., Sun, X., and Hoeksema, J.T.: 2012, *Solar Phys.* **281**, 37.
- Zaitsev, V.V., Kronshtadtov, P.V., and Stepanov, A.V.: 2016, *Solar Phys.* **291**, 3451.
- Zimovets, I.V. and Struminsky, A.B.: 2009, *Solar Phys.* **258**, 69.
- Zimovets, I.V., Kuznetsov, S.A., and Struminsky, A.B.: 2013, *Astronomy Letters* **39**, 267.

**Table 1.** Geometrical characteristics of the reconstructed MFRs ( $L_{\text{MFR}}$  and  $H_{\text{MFR}}$ ), characteristics of the HXR pulsations ( $n_p$  and  $\langle P \rangle$ ) and two different classifications of the flares studied

1	2	3	4	5	6	7
Flare	$L_{\text{MFR}}$ , Mm	$H_{\text{MFR}}$ , Mm	$n_p$	$\langle P \rangle$ , s	group	case
15-Feb-2011	44	14	35	16	2	a
07-Jun-2011	46	13	36	26	1	b
06-Sep-2011	25	9	20	21	1	b
18-Apr-2014	46	31	23	24	2	b
22-Oct-2014	64	20	10	21	1	b
24-Oct-2014	134	31	34	17	2	a
09-Nov-2014	24	6	8	20	1	a

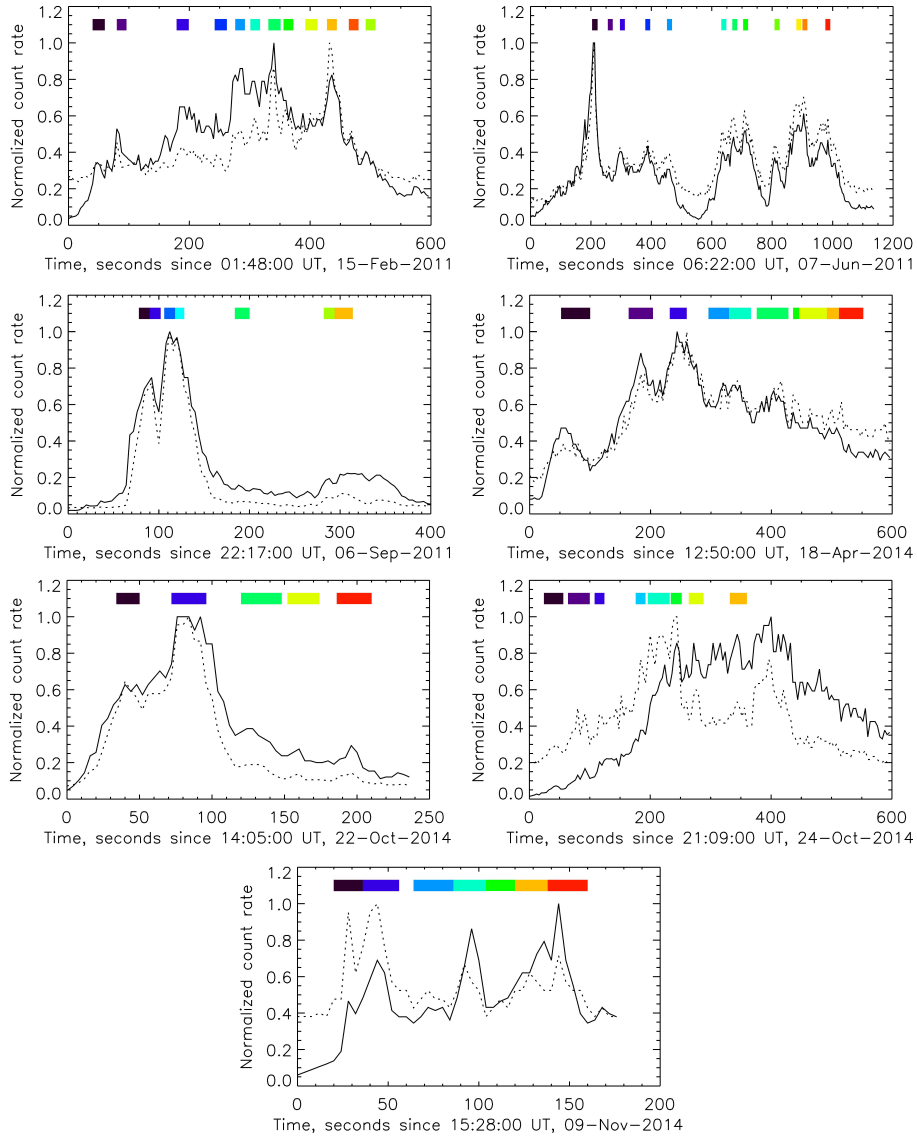


**Figure 1.** Normalized (to the maximum) four-second RHESSI corrected count rates in the 25–50 keV (solid curves) and 50–100 keV (dotted curves) energy channels, for seven solar flares studied. The color horizontal segments at the top mark the time intervals of different HXR pulsations for which the HXR images were synthesized and positions of the HXR sources were found for the further analysis. These time intervals (and corresponding colors) almost coincide with the time intervals (and corresponding colors) determined in Paper I. Spatial positions of the centers of maximum brightness of these HXR sources are used as the starting points in the chromosphere for the reconstruction of the magnetic field lines shown in Figures 2–3 by appropriate colors.

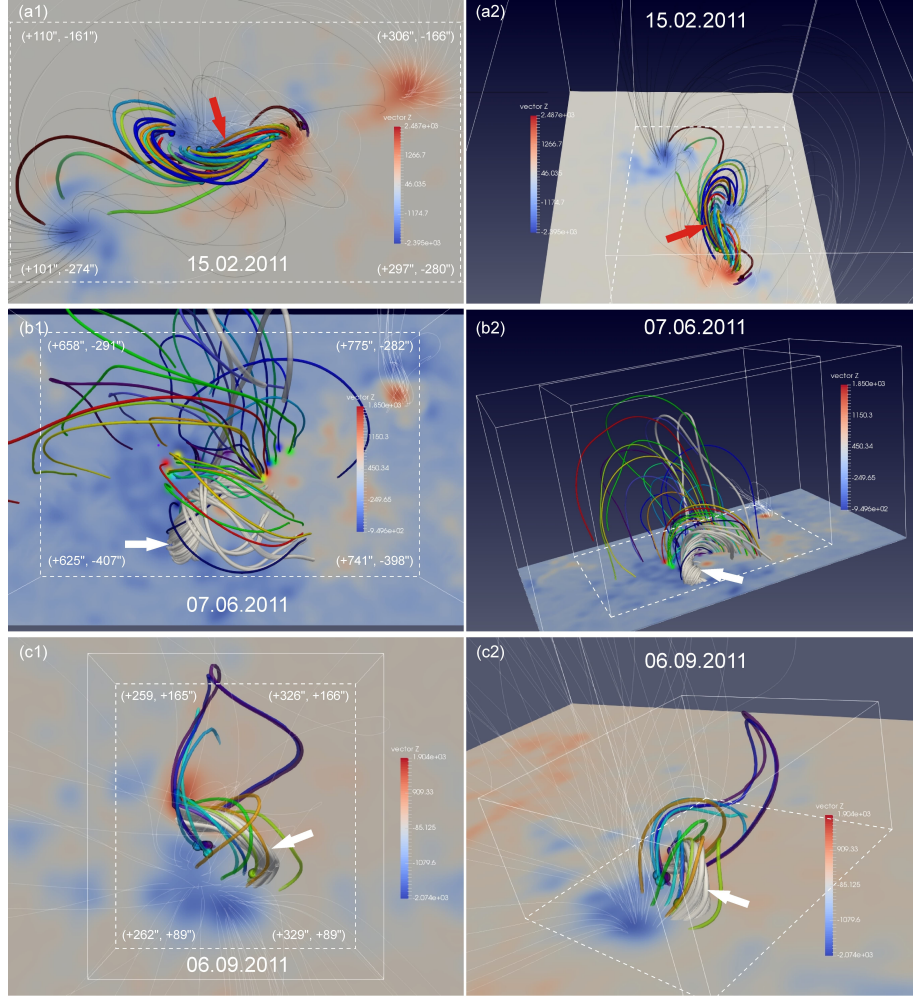


**Figure 2.** Reconstructed magnetic field lines in the regions of the 15-Feb-2011 (a), 07-Jun-2011 (b) and 06-Sep-2011 (c) solar flares accompanied by the HXR (25–50 keV) pulsations (see Figure 1). The top view is on the left, the side view is on the right. Colors of the field lines correspond to the colors of the sources of the HXR pulsations (see Figure 1; the spatial locations of these HXR sources are also shown in Paper I). The HXR sources (*i.e.* the positions of their brightness maxima) are shown here by small circles of the appropriate colors. The twisted bundles of the thick light gray field lines represent a magnetic flux rope (MFR) found in the core of these flare regions. The MFR is also indicated by the thick white arrow. The red arrow indicates the MFR composed of the field lines (colored) reconstructed from the sources of the HXR pulsations. Thin gray field lines are background magnetic field lines started from the strongest nearby magnetic sources. The background images are the maps of the radial magnetic field component ( $B_r$ ) on the photosphere made with the pre-flare SDO/HMI magnetograms (SHARPs). The colorbars show values of  $B_r$  for the corresponding colors. The thin white dashed quadrangles left and right on the photosphere are shown just to indicate the regions of interest and to give the reference helioprojective cartesian coordinates (HPC) of its corners (in arcseconds).

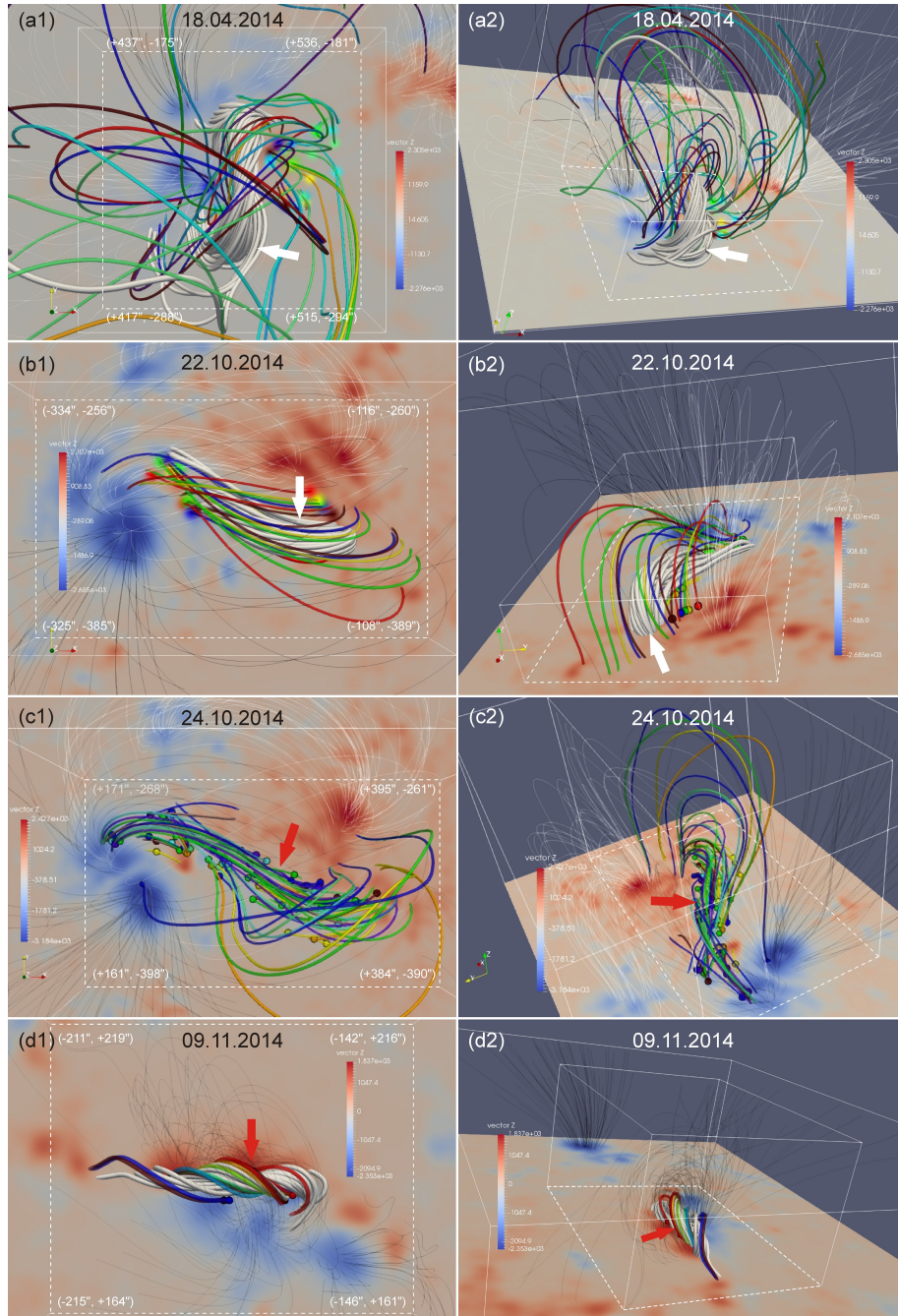


**Figure 3.** Reconstructed magnetic field lines in the regions of the 18-Apr-2014 (a), 22-Oct-2014 (b), 24-Oct-2014 (c) and 09-Nov-2014 (d) solar flares accompanied by the HXR pulsations. The same notations as in Figure 2.

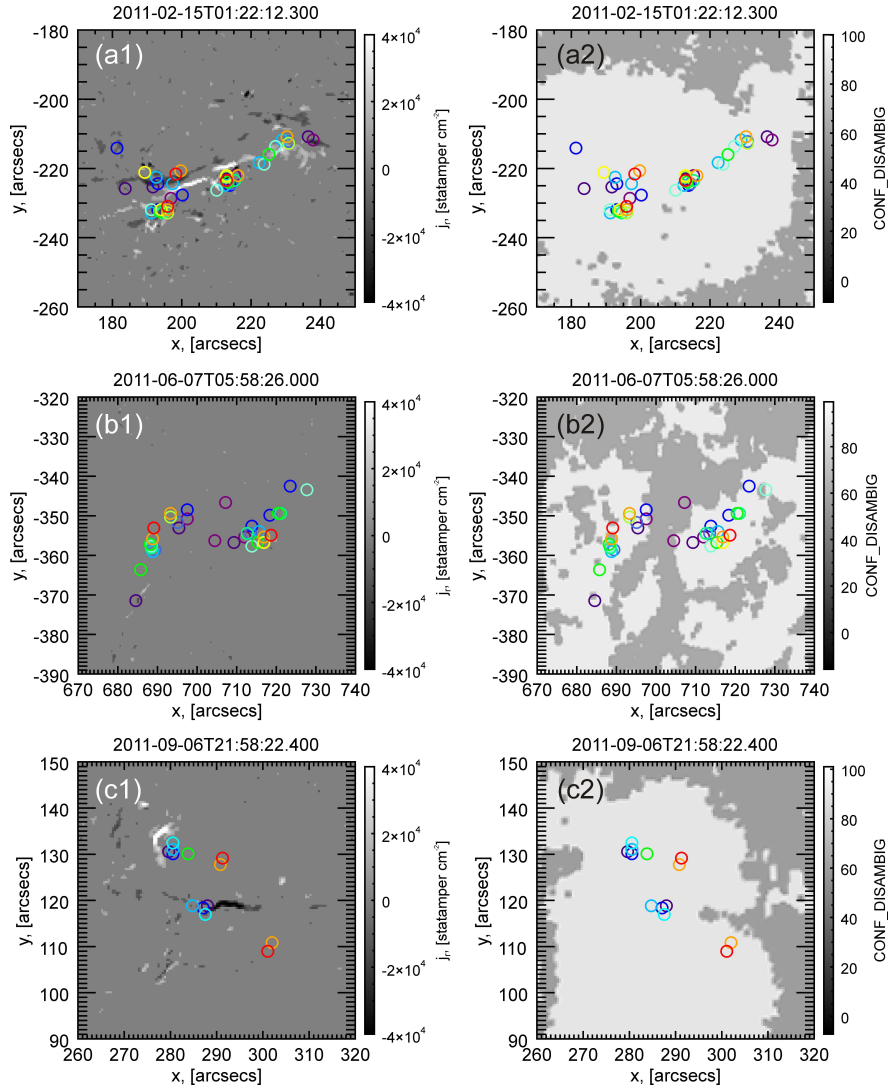


**Figure 4.** Spatial relationship of the sources of the HXR pulsations (25–50 keV) and vertical electric current density ( $j_r$ ) on the photosphere in the regions of the 15-Feb-2011 (a), 07-Jun-2011 (b) and 06-Sep-2011 (c) solar flares. The centers of maximum brightness of the HXR sources of different pulsations are shown by the circles of the appropriate colors (see Figures 2–3 above and figures in Paper I). (*Left*) Pre-flare maps of  $j_r$ . The color scale (see the colorbars on the right) is restricted artificially by the values of  $j_r^{\min} = -4 \times 10^4$  statampere  $\text{cm}^{-2}$  and  $j_r^{\max} = +4 \times 10^4$  statampere  $\text{cm}^{-2}$  for higher contrast. (*Right*) Pre-flare maps of the confidence level assigned to the final disambiguation solution for each pixel of the SDO/HMI vector magnetograms (SHARPs) used. The observational times of the magnetograms are shown above each figure.

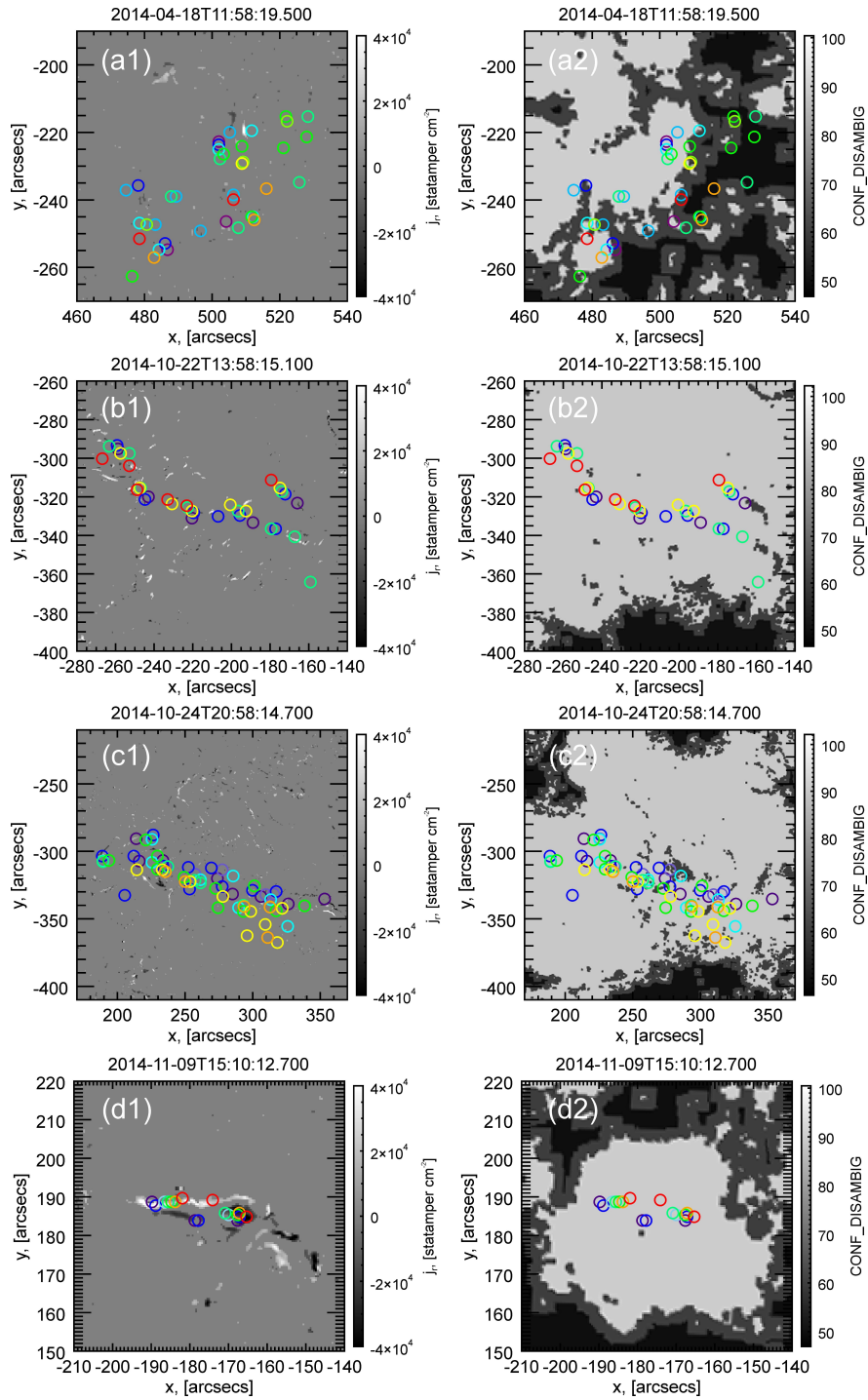


**Figure 5.** Spatial relationship of the sources of the HXR pulsations (25–50 keV) and vertical electric current density ( $j_r$ ) on the photosphere in the regions of the 18-Apr-2014 (a), 22-Oct-2014 (b), 24-Oct-2014 (c) and 09-Nov-2014 (d) solar flares. The same notations as on Figure 4.

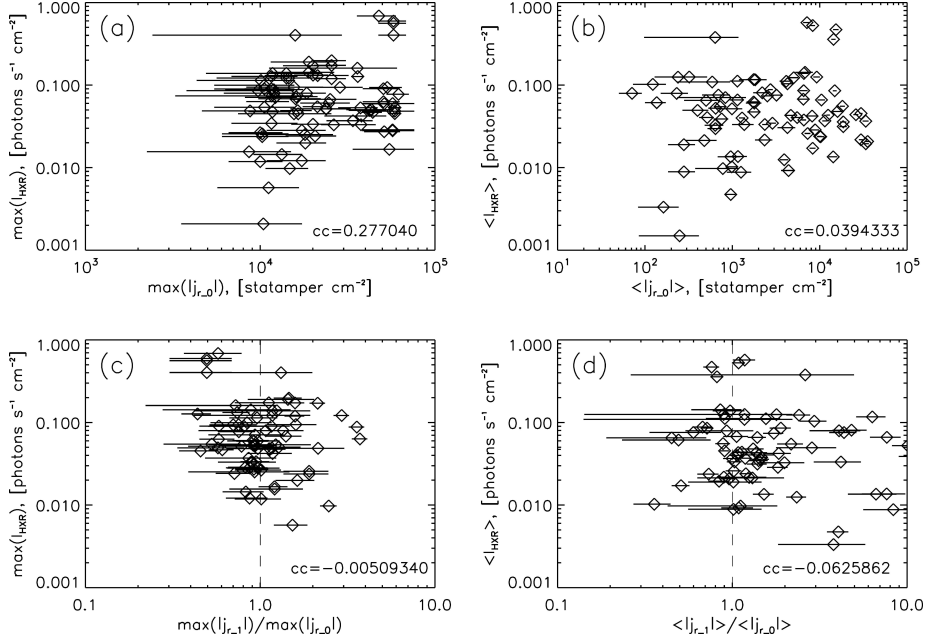


**Figure 6.** Dependencies of the flux of the sources of the HXR pulsations ( $I_{\text{HXR}}$ ) on the vertical electric current density ( $j_r$ ) on the photosphere below the HXR sources for all seven solar flares studied. Only data points with  $j_r$  values above the error threshold level are shown (see text). (a) Dependence of the brightest pixel flux of the HXR sources ( $\max(I_{\text{HXR}})$ ) on the maximum absolute value of pre-flare electric current density ( $\max(j_{r,0})$ ) below the HXR sources. (b) Dependence of the mean flux of the HXR sources ( $\langle I_{\text{HXR}} \rangle$ ) on the mean absolute value of pre-flare electric current density ( $\langle |j_{r,0}| \rangle$ ) below the HXR sources. (c) Dependence of the brightest pixel flux of the HXR sources on the ratio of maximum absolute values of post-flare ( $\max |j_{r,1}|$ ) and pre-flare ( $\max |j_{r,0}|$ ) electric current densities below the HXR sources. (d) Dependence of the mean flux of the HXR sources on the ratio of the mean absolute values of the post-flare and pre-flare electric current densities below the HXR sources. The values of the linear Pearson correlation coefficient ( $cc$ ) are shown in the right bottom corners.

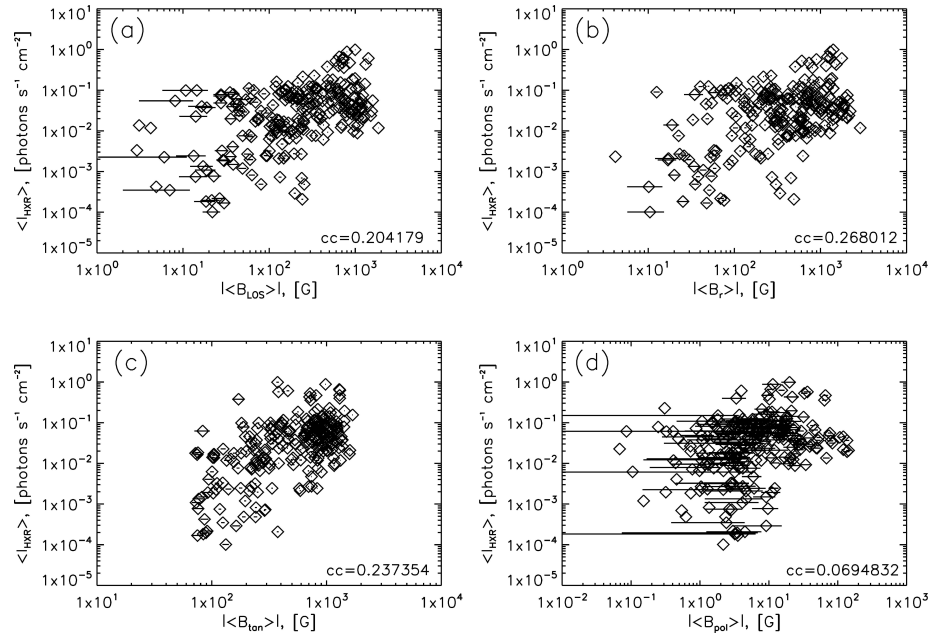


**Figure 7.** Dependencies of the mean flux of the sources of the HXR pulsations ( $\langle I_{\text{HXR}} \rangle$ ) on the absolute mean values of pre-flare magnetic field components on the photosphere below the HXR sources: (a) line-of-sight component ( $B_{\text{los}}$ ), (b) radial (vertical) component ( $B_r$ ); (c) tangential (to the solar surface) component ( $B_{\text{tan}}$ ); (d) poloidal component ( $B_{\text{pol}}$ ). The values of the linear Pearson correlation coefficient ( $cc$ ) are shown in the right bottom corners.

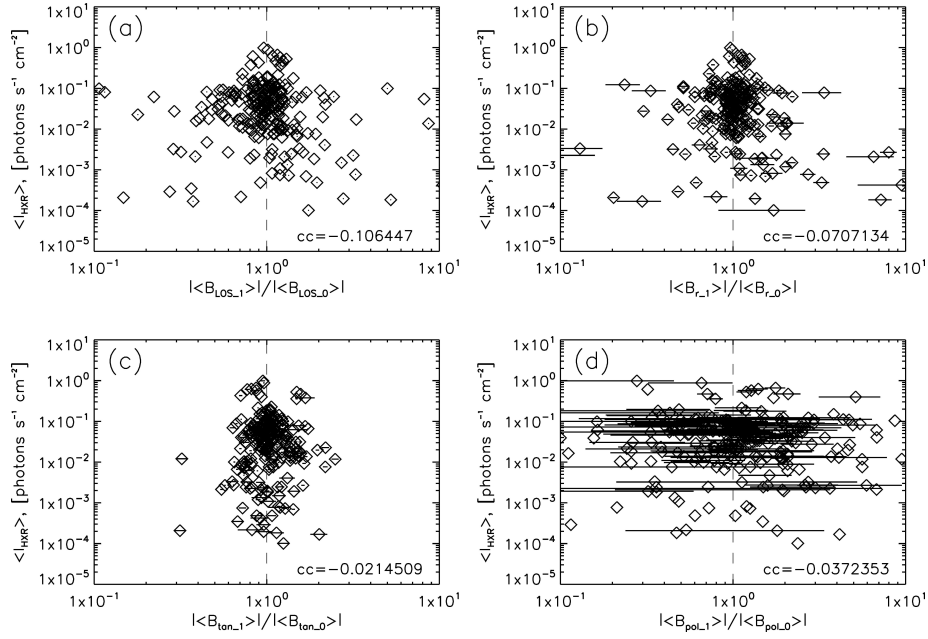


**Figure 8.** Dependencies of the mean flux of the sources of the HXR pulsations ( $\langle I_{\text{HXR}} \rangle$ ) on the ratio of the absolute mean values of post- (subscript “1”) and pre-flare (subscript “0”) magnetic field components on the photosphere below the HXR sources: (a) line-of-sight component ( $B_{\text{los}}$ ), (b) radial (vertical) component ( $B_r$ ); (c) tangential (to the solar surface) component ( $B_{\text{tan}}$ ); (d) poloidal component ( $B_{\text{pol}}$ ). The values of the linear Pearson correlation coefficient ( $cc$ ) are shown in the right bottom corners.

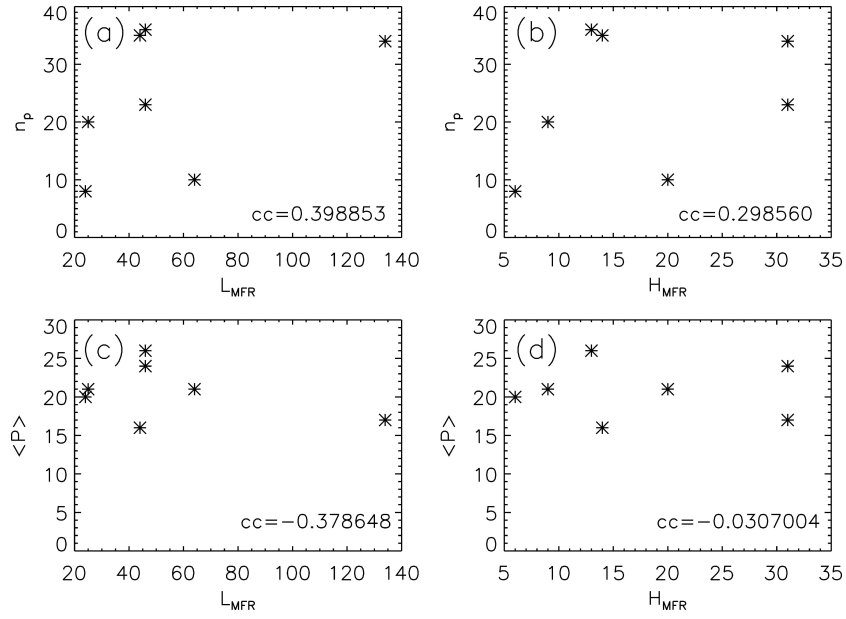


**Figure 9.** Scatter plots of characteristics of the HXR pulsations ( $n_p$  and  $\langle P \rangle$ ) and geometrical characteristics of the reconstructed magnetic flux ropes ( $L_{MFR}$  and  $H_{MFR}$ ). The values of the linear Pearson correlation coefficient ( $cc$ ) are shown in the right bottom corners.